Synthesis, Structure and Aromaticity of Metallapyridinium Complexes

Yilun Wang[†],[a,b] Yue Sun[†],[a] Wei Bai,*[a] Yan Zhou,[c] Xiao Bao,[a] and Yang Li*[a,b]

[a] State Key Laboratory of Fine Chemicals, Department of Chemistry, School of Chemical Engineering, Dalian University of Technology, Liaoning 116024, P.R. China

[b] School of Chemical Engineering, Dalian University of Technology, Panjin, Liaoning 124221, P.R. China

[c] School of Chemistry and Chemical Engineering, Guangxi University for Nationalities, Guangxi Key Laboratory of Chemistry and Engineering of Forest Products, Key Laboratory of Guangxi Colleges and Universities for Food Safety and Pharmaceutical Analytical Chemistry, Nanning, 530008, P.R. China

Supporting Information

Table of Contents

1.Computational details

All the optimizations were performed with the Gaussian 16 software package.[1] All of these structures evaluated were optimized at the B3LYP level of density functional theory (DFT).[2] DFT/GENECP level had been done by implementing def2-TZVP basis set for Re atom.[3] On the other hand, 6-311G(2d,p) basis set had been used for the rest of atoms.[4] Nucleus-independent chemical shift (NICS) values were calculated at the B3LYP-GIAO//6-311G(2d,p)/def2-TZVP level, whereas we performed the CMO-NICS calculations in simplified models with the NBO 7.0 program.[5] The iso-chemical shielding surface (ICSS) is a method closely related to NICS. It calculates the grid point data of magnetic shielding value in three-dimensional space and draws the contour map. The $ICSS_{ZZ}$ is a real space function, which can clearly show the shielding or deshielding effect of the external magnetic field in the direction perpendicular to the ring. Unlike the $NICS_{ZZ}$ values, the positive value of $ICSS_{ZZ}$ indicates the shielding effect of the external magnetic field at this point, and the absolute values of the two parameters are the same. The anisotropy of the current density was calculated with the AICD 2.0 program computing the NMR properties using the CSGT method with the Gaussian16 Rev A.03 program with the geometries previously obtained for **M-N** and **M-N-H**.[6] GIMIC analysis was finished by GIMIC code [7] based on the formatted check point file of Gaussian and rendered by ParaView visualization program.[8] Using RunEDDB script,[9] electron density of delocalized bond (EDDB) [10] based on natural atomic orbitals (NAOs) is analyzed. The molecular orbital composition and MO pictures were analyzed using Multiwfn, a multifunctional wavefunction analyzer.[11] The calculations of MCI and ELFπ were also carried out by Multiwfn package. If the MCI value is high and the difference in the bifurcation value ($\Delta BV(ELF_{\pi})$) is small, then the π electrons should be highly delocalized and the species should be aromatic. The MO pictures were drawn using the software of VMD.[12] VMD was developed by the Theoretical and Computational Biophysics Group in the Beckman Institute for Advanced Science and Technology at the University of Illinois at Urbana-Champaign (http://www.ks.uiuc.edu/Research/vmd/).

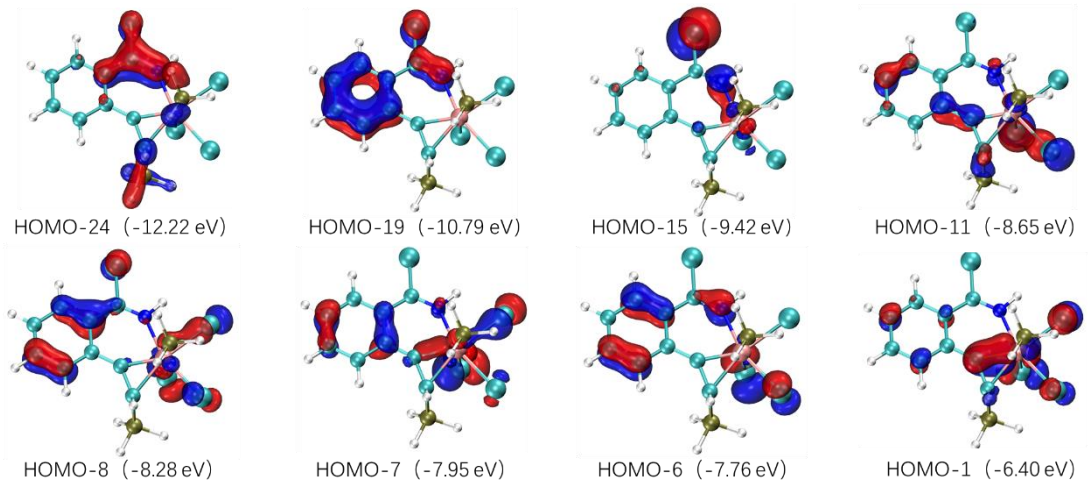

Figure S1. Key occupied π-MOs of **M-N**. The isosurface of MOs is 0.04.

Table S1. Full Cartesian NMR shielding tensor (ppm) for NICS values of π-Canonical MO contributions in **M-N** ($NICS(1)_{zz}$ and $NICS(-1)_{zz}$ are the $NICS(1)_{zz}$ values of the upper and lower directions of the rings, respectively. Orbital 93 is HOMO).

MO	$NICS(0)_{zz}$ for **3MR**	$NICS(0)_{zz}$ for **6MR**	$NICS(1)_{zz}$ for **3MR**	$NICS(-1)_{zz}$ for **3MR**	$NICS(1)_{zz}$ for **6MR**	$NICS(-1)_{zz}$ for **6MR**
69	3.94	6.05	3.6	3.69	4.85	5.43
74	3.38	6	3.11	2.85	5.08	5.05
78	2.09	2.27	2.19	1.44	2.15	1.82
82	-4.95	-0.17	-3.65	-3.8	-0.01	-0.15
85	0.72	-3.45	0.87	-0.27	-3.86	-1.81
86	-0.75	-2.58	-2.1	-2.28	-1.15	-1.91
87	-3.67	-3.73	-3.04	-1.53	-3.37	-2.89
92	-5.19	-1.32	-4.27	-5.88	-0.78	-1.51
sum	-4.43	3.07	-3.29	-5.78	2.91	4.03

The signs of the NICS values are reversed from those of the shielding data in the output. Thus, the NICS value is the negative of the sum of the shielding contributions.

Thus, NICS(0)$_{ZZ}$-π value of **3MR** is +4.43 ppm; NICS(0)$_{ZZ}$-π value of **6MR** is -3.07 ppm; NICS(1)$_{ZZ}$-π value of **3MR** is the mean value of NICS(1)$_{ZZ}$-π and NICS(-1)$_{ZZ}$-π: -(-3.29 – 5.78) / 2 = 4.535 ppm; NICS(1)$_{ZZ}$-π value of **6MR** is -3.47 ppm.

Table S2. Full Cartesian NMR shielding tensor (ppm) for NICS values of σ-Canonical MO contributions in **M-N** (NICS(1)$_{ZZ}$ and NICS(-1)$_{ZZ}$ are the NICS(1)$_{ZZ}$ values of the upper and lower directions of the rings, respectively）.

MO	NICS (0)$_{ZZ}$ for **3MR**	NICS (0)$_{ZZ}$ for **6MR**	NICS(1)$_{ZZ}$ for **3MR**	NICS(-1)$_{ZZ}$ for **3MR**	NICS(1)$_{ZZ}$ for **6MR**	NICS(-1)$_{ZZ}$ for **6MR**
45	4.79	8.72	4.31	3.77	5.35	5.54
46	4.19	6.22	4.13	3.85	5.25	5.25
47	1.14	1.75	1	0.96	0.95	1.03
48	7.19	4.43	5.31	4.18	3.67	3.52
49	3.34	6.12	3.31	2.91	4.19	4.21
50	3.85	2.7	3.35	2.67	2.39	2.27
51	1.41	0.41	1.02	0.6	0.38	0.34
52	0.64	0.63	0.68	0.45	0.57	0.52
53	0.63	0.36	0.24	0.31	0.42	0.46
54	4.56	2.57	2.29	2.69	2.41	2.19
55	1.57	1.68	0.95	2.61	1.18	2.42
56	4.13	3.7	2.74	2.58	2.78	2.76
57	3.58	4.52	2.56	2.4	2.87	2.77
58	2.14	1.3	1.73	1.62	2.23	2.15
59	3.42	1.94	2.27	1.76	2.01	1.83
60	2.67	1.67	0.19	-0.31	1.61	1.53
61	3.72	5.1	2.67	2.2	3.05	3.17
62	-1.61	-3.3	-1.34	-1.53	-1.52	-1.41
63	2.02	1.73	1.76	1.42	1.69	1.9
64	-3.13	-4.75	-2.68	-2.61	-2.47	-2.74

65	0.63	0.89	-1.13	0.66	0.98	0.7
66	-0.23	-0.27	-1.09	0.08	-0.35	-0.21
67	-0.6	-4.67	-1.37	-0.29	-3.03	-3.04
68	2.47	3.09	2.1	1.35	2.68	2.74
70	-0.14	0.36	0.1	-0.91	0.43	-0.14
71	0.83	-0.24	0.69	1.11	0.03	-0.95
72	3.76	-9.9	1	1.15	-4.98	-4.93
73	-3.64	-6.44	-4.33	-4.24	-5.04	-4.88
75	-4.34	-5.58	-3.78	-3.4	-3.87	-4.04
76	-2.84	-5.58	-4.03	-3.83	-4.25	-4.29
77	-5.59	-9.7	-1.52	-1.89	-3.57	-4.19
79	-2.61	-5.64	-1.81	-1.48	-3.4	-3.59
80	2.54	2.76	1.67	1.97	2.13	2.39
81	10.8	-3.73	4.91	4.26	-0.86	-0.91
83	-3.37	-4.5	-4.22	-4.36	-2.76	-2.59
84	2.31	-10.7	-1.26	1.11	-6.55	-6.93
89	-2.16	-4.91	0.62	-0.48	-3.3	-2.75
91	0.07	-3.6	-2.83	-4.14	-3.39	-2.94
sum	48.14	-20.86	20.21	19.2	-0.09	-0.84

The signs of the NICS values are reversed from those of the shielding data in the output. Thus, the NICS value is the negative of the sum of the shielding contributions. Thus, $NICS(0)_{ZZ}$-σ value of **3MR** is -48.14 ppm; $NICS(0)_{ZZ}$-σ value of **6MR** is 20.86 ppm; $NICS(1)_{ZZ}$-σ value of **3MR** is the mean value of $NICS(1)_{ZZ}$-σ and $NICS(-1)_{ZZ}$-σ: -(20.21 + 19.2) / 2 = -19.705 ppm; $NICS(1)_{ZZ}$-σ value of **6MR** is -0.465 ppm.

Table S3. The positive and negative values of total induced currents contributed by the diatropic and paratropic currents

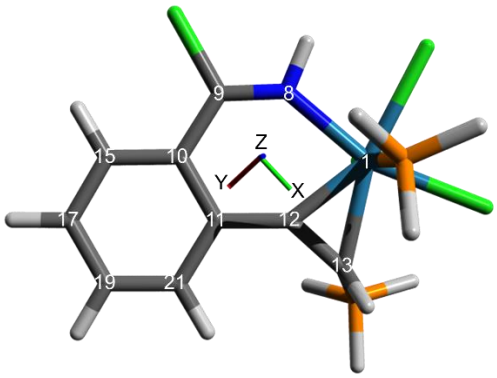

Bond	diatropic contribution	paratropic contribution	Total induced current
1-8	14.155874	-6.941062	7.214812
8-9	14.759157	-6.163534	8.595624
9-10	11.934445	-4.043308	7.891137
10-15	15.908407	-5.260412	10.647995
15-17	16.625262	-4.977776	11.647486
17-19	16.436973	-4.803325	11.633647
19-21	16.521090	-4.745870	11.775220
21-11	15.882286	-4.963869	10.918416
11-12	13.362162	-5.417693	7.944470
12-13	12.811744	-0.139580	12.672165
13-1	11.647764	-0.542425	11.105340

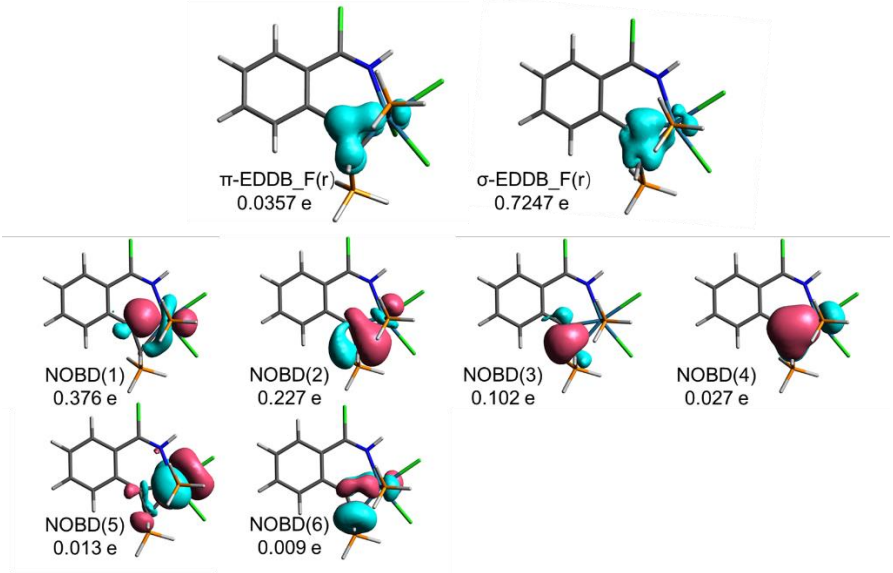

Figure S2. EDDB_F(r) results for the **3MR** in **M-N** and key NOBDs of the ring. Isovalues are 0.0003, 0.008 for π-EDDB_F(r), σ-EDDB_F(r), respectively. Isovalue for NOBD contours is 0.040.

Natural orbitals for bond delocalization (NBODs) computed for the **3MR** indicate that the main σ bondings (NOBD(1−3, 5) in Figure S2) between the metal center and two carbon atoms account for the σ-electron delocalization involving in-plane overlap of metal d and carbon p orbitals; whereas the π delocalization is minor, as shown in NOBD(4, 6).

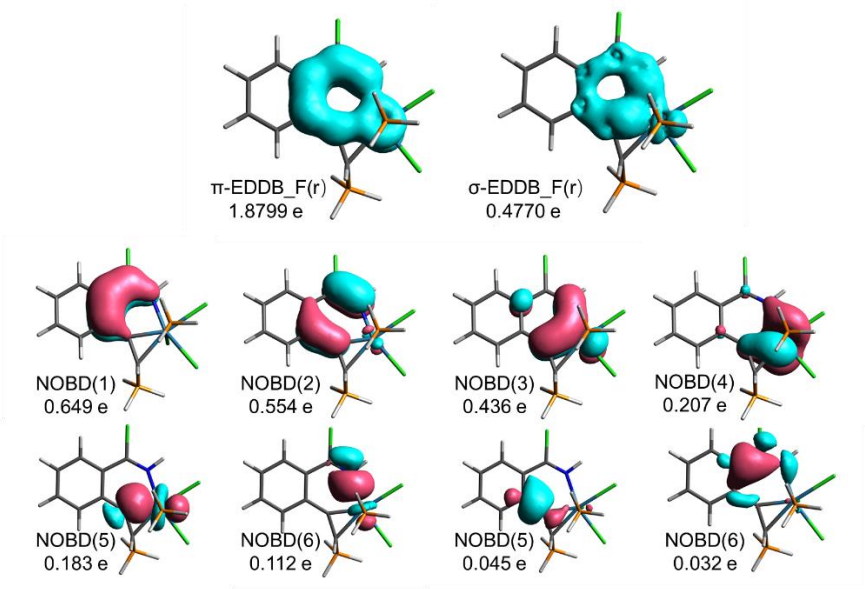

Figure S3. EDDB_F(r) results for the **6MR** in **M-N** and key NOBDs of the ring. Isovalues are 0.005, 0.004 for π-EDDB_F(r), σ-EDDB_F(r), respectively. Isovalue for NOBD contours is 0.040.

Natural orbitals for bond delocalization (NBODs) computed for the **6MR** indicate that the π delocalization is major (as shown in NOBD(1-4)).

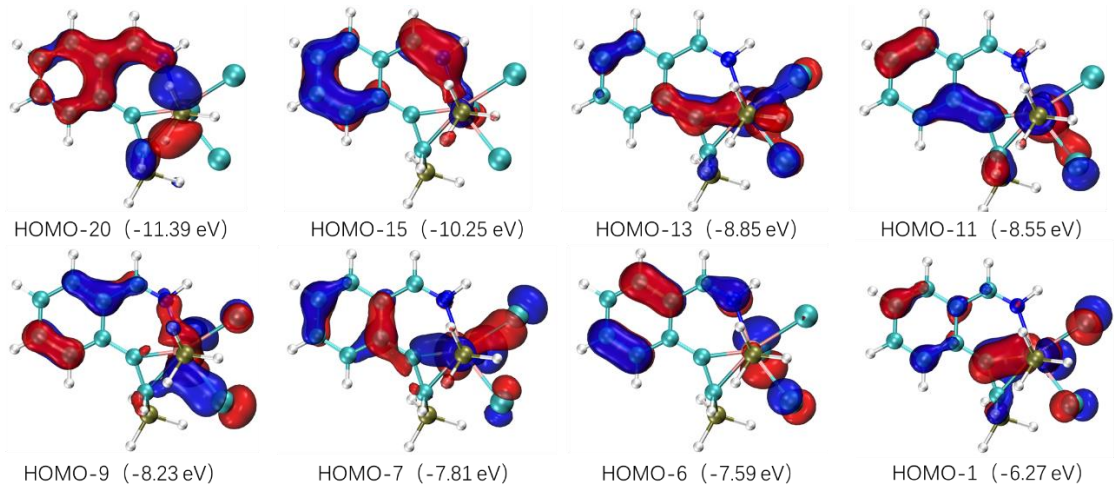

Figure S4. Key occupied π-MOs of **M-N-H**. The isosurface of MOs is 0.04.

Table S4. Full Cartesian NMR shielding tensor (ppm) for NICS values of π-Canonical MO contributions in **M-N-H** ($NICS(1)_{zz}$ and $NICS(-1)_{zz}$ are the $NICS(1)_{zz}$ values of the upper and lower directions of the rings, respectively. Orbital 85 is HOMO).

MO	$NICS(0)_{zz}$ for **3MR**	$NICS(0)_{zz}$ for **6MR**	$NICS(1)_{zz}$ for **3MR**	$NICS(-1)_{zz}$ for **3MR**	$NICS(1)_{zz}$ for **6MR**	$NICS(-1)_{zz}$ for **6MR**
65	3.08	4.77	2.99	2.38	4.18	3.67
70	4.12	6.45	3.13	3.8	5.45	5.2
72	2.46	2.81	1.77	1.84	2.25	2.42
74	-4.12	-0.19	-3.36	-2.93	-0.08	-0.28
76	0.02	-0.46	-2.09	1.89	-0.31	-0.01
78	-0.13	-2.98	-1.32	-1.83	-1.31	-2.21
79	-4.46	-3.9	-4	-2.22	-3.46	-3.07
84	-5.52	-0.73	-4.6	-6.21	-0.26	-1
sum	-4.55	5.77	-7.48	-3.28	6.46	4.72

The signs of the NICS values are reversed from those of the shielding data in the output. Thus, the NICS value is the negative of the sum of the shielding contributions.

Thus, NICS(0)$_{ZZ}$-π value of **3MR** is 4.55 ppm; NICS(0)$_{ZZ}$-π value of **6MR** is -5.77 ppm; NICS(1)$_{ZZ}$-π value of **3MR** is the mean value of NICS(1)$_{ZZ}$-π and NICS(-1)$_{ZZ}$-π: -(-7.48-3.28) / 2 = 5.38 ppm; NICS(1)$_{ZZ}$-π value of **6MR** is -5.59 ppm.

Table S5. Full Cartesian NMR shielding tensor (ppm) for NICS values of σ-Canonical MO contributions in **M-N-H** (NICS(1)$_{ZZ}$ and NICS(-1)$_{ZZ}$ are the NICS(1)$_{ZZ}$ values of the upper and lower directions of the rings, respectively）.

MO	NICS (0)$_{ZZ}$ for **3MR**	NICS (0)$_{ZZ}$ for **6MR**	NICS(1)$_{ZZ}$ for **3MR**	NICS(-1)$_{ZZ}$ for **3MR**	NICS(1)$_{ZZ}$ for **6MR**	NICS(-1)$_{ZZ}$ for **6MR**
40	5.66	10.1	5.06	4.45	6.1	6.3
41	4.25	6.07	4.17	3.88	5.12	5.18
42	7.18	4.81	5.47	4.33	3.93	3.75
43	3.3	5.85	3.2	2.98	4.31	4.46
44	4.12	3.03	3.58	2.8	2.53	2.4
45	1.38	0.44	1.02	0.6	0.4	0.35
46	0.67	0.64	0.69	0.47	0.59	0.55
47	0.69	0.35	0.27	0.34	0.42	0.46
48	4.24	2.67	2.18	2.6	2.43	2.24
49	1.67	1.79	0.99	2.65	1.31	2.46
50	4.17	3.53	2.46	2.38	2.93	2.94
51	3.82	5.3	2.91	2.7	3.14	3.09
52	2.64	2.52	2.08	1.89	2.84	2.77
53	3.33	1.74	2.12	1.56	1.72	1.54
54	3.01	3.89	2.75	2.41	2.64	2.68
55	3.96	3.6	0.97	0.29	2.63	2.61
56	-1.56	-2.67	-1.28	-1.54	-1.15	-0.94
57	2.9	2.08	2.35	2.77	2.15	2.07
58	-0.9	-3.09	-0.78	-0.93	-1.74	-2.02
59	-3.23	-3.16	-2.94	-2.2	-2.54	-2

60	1.52	1.04	-1.47	0.57	1.28	0.78
61	-2.55	-6.02	-2.88	-1.94	-3.98	-3.97
62	1.25	1.12	1.1	0.37	1.04	1.12
63	2.66	4.05	2.21	2.88	3.19	3.9
64	0.61	-0.28	0.67	0.16	0.02	-1.08
66	4.44	-9.73	1.33	1.59	-5.29	-5.27
67	-3.15	-6.65	-4.21	-4.13	-4.78	-4.69
68	-5.25	-7.68	-4.65	-4.65	-5.45	-5.66
69	-0.32	-4	-1.7	-2.94	-2.88	-2.78
71	-10.25	-13.91	-3.65	-3.36	-5.63	-6.7
73	10.31	-3.92	4.73	4.04	-0.93	-0.95
75	-3.76	-4.41	-2.92	-5.25	-2.56	-2.61
77	3.88	-12.13	1.43	0.42	-8.51	-6.67
81	-2.14	-4.82	0.63	-0.39	-3.24	-2.7
83	0.08	-3.57	-2.9	-4.19	-3.34	-2.96
sum	48.63	-21.42	24.99	17.61	-1.3	0.65

The signs of the NICS values are reversed from those of the shielding data in the output. Thus, the NICS value is the negative of the sum of the shielding contributions. Thus, NICS(0)$_{ZZ}$-σ value of **3MR** is -48.63 ppm; NICS(0)$_{ZZ}$-σ value of **6MR** is 21.42ppm; NICS(1)$_{ZZ}$-σ value of **3MR** is the mean value of NICS(1)$_{ZZ}$-σ and NICS(-1)$_{ZZ}$-σ: -(24.99 + 17.61) / 2 = -21.3 ppm; NICS(1)$_{ZZ}$-σ value of **6MR** is 0.325ppm.

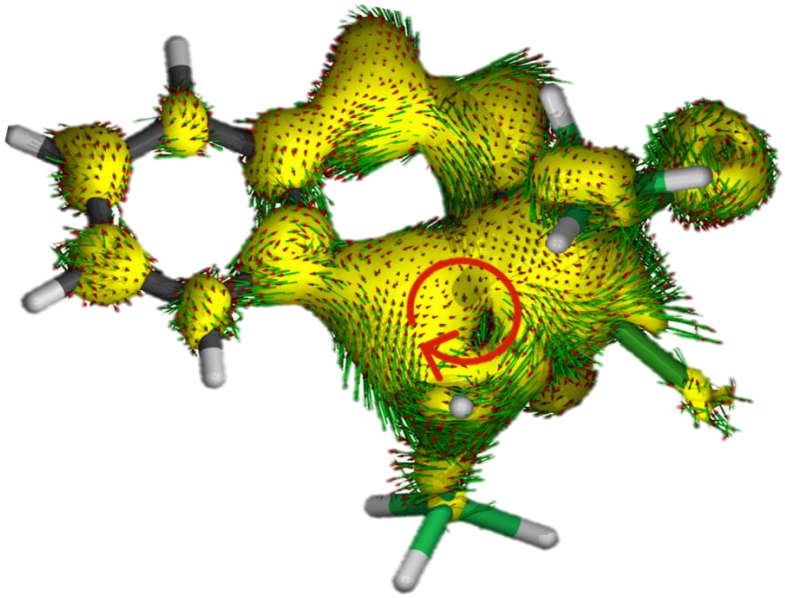

Figure S5. AICD isosurfaces of **M-N-H** separated into the σ-contribution (current density vectors are plotted onto the AICD isosurface of 0.030 and the magnetic field vector is orthogonal with respect to the ring plane and points upward (clockwise currents are diatropic).

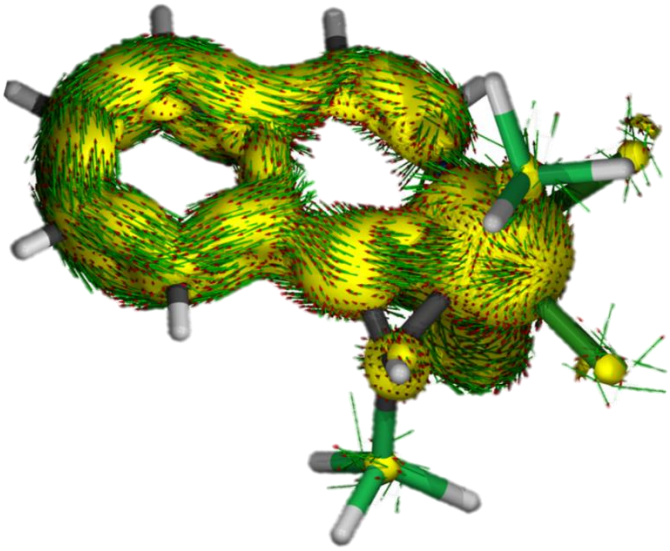

Figure S6. AICD isosurfaces of **M-N-H** separated into the π-contribution (current density vectors are plotted onto the AICD isosurface of 0.030 and the magnetic field vector is orthogonal with respect to the ring plane and points upward (clockwise currents are diatropic).

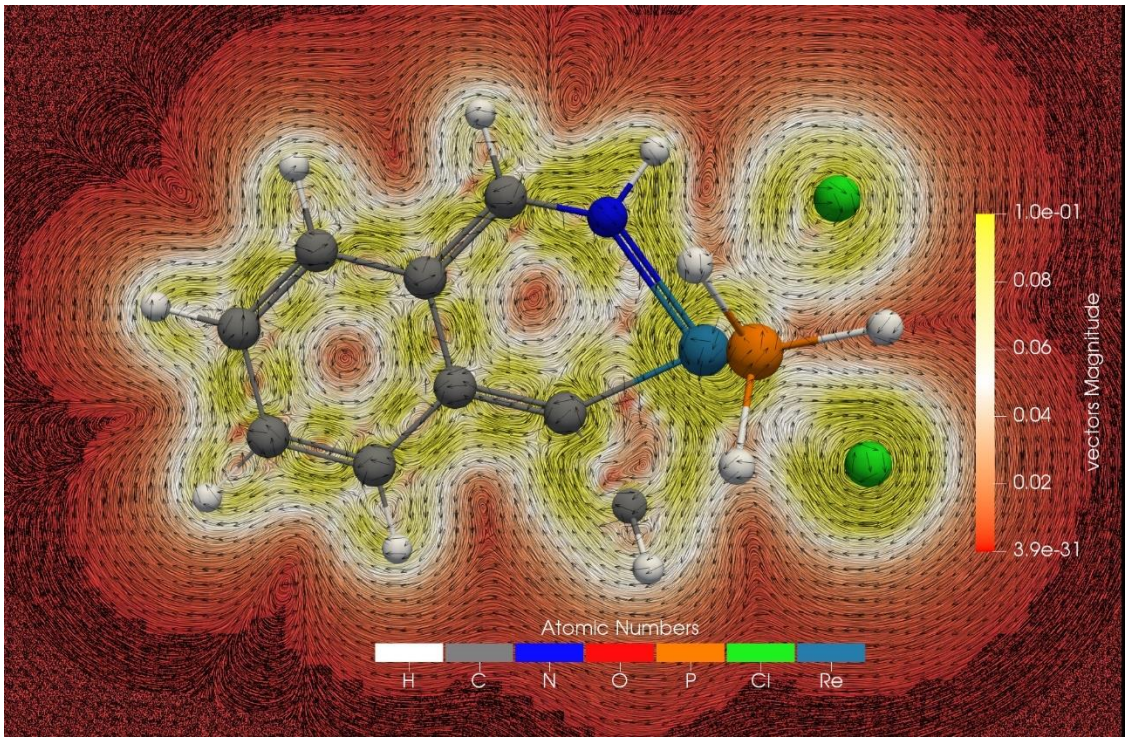

Figure S7. GIMIC map in the plane of **6MR** in **M-N-H**. In both maps, the magnetic field vector is orthogonal with respect to the ring plane and points upward (clockwise currents are diatropic).

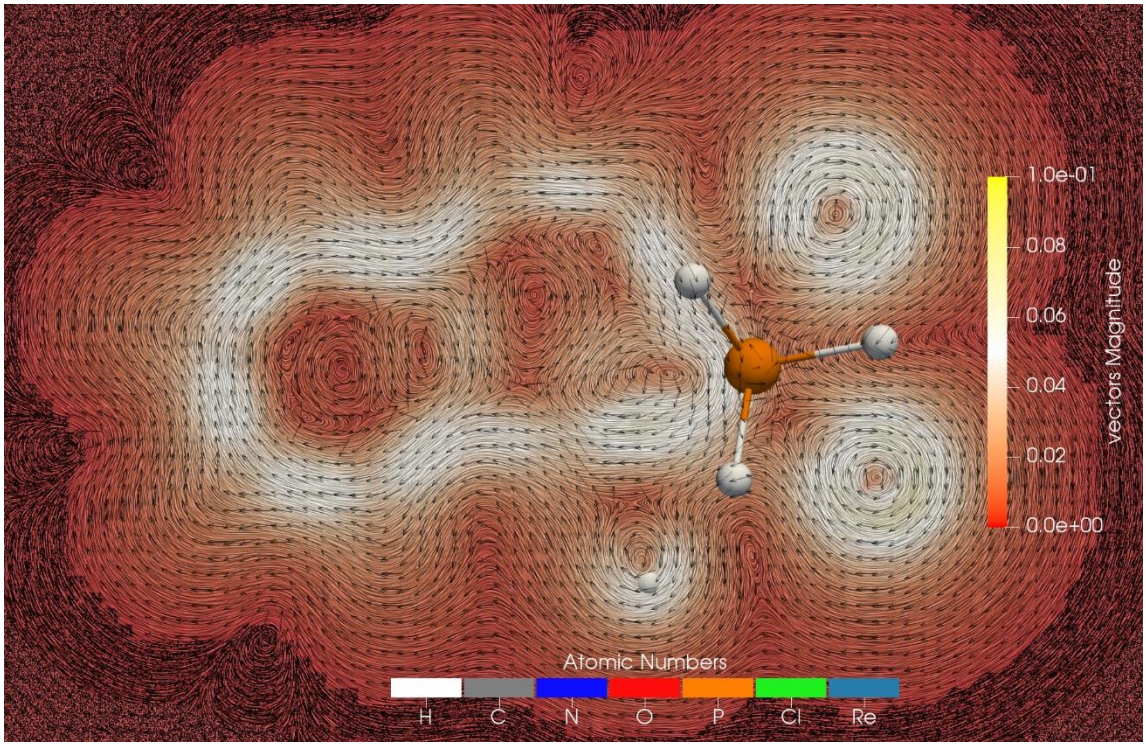

Figure S8. GIMIC map (1.5 Bohr above the **6MR**) in **M-N-H**. In both maps, the magnetic field vector is orthogonal with respect to the ring plane and points upward (clockwise currents are diatropic).

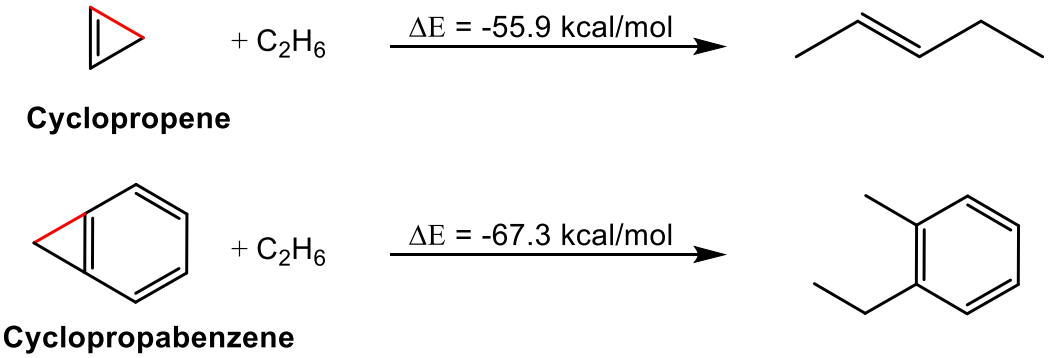

Figure S9. Isodesmic reactions for some non-metallic rings.

2. X-ray crystallographic study of complex 2 and $4^{+}(BPh_4^{-})$

Table S6. Crystallographic data and refinement details for **2** and $\mathbf{4^{+}(BPh_4^{-})}$

	2	$\mathbf{4^{+}(BPh_4^{-})}$
CCDC Number	2045090	2081090
Empirical formula	C35H32Cl4NP2Re	C75H71BCl3NOP3Re
Color & habit	red, block	red, block
Crystal size (mm^3)	0.20 x 0.15 x 0.10	0.35 x 0.20 x 0.10
Temperature (K)	173K	190K
Crystal system	Monoclinic	Monoclinic
Space group	$P2_1/c$	$P2_1/c$
a(Å)	17.0191(9)	19.2784(8)
b(Å)	11.9932(6)	22.0302(9)
c(Å)	17.2230(9)	17.0720(7)
	90	90
	108.585(2)	106.1640(10)
	90	90
V($Å^3$), Z	3332.1(3), 4	6964.0(5), 4
D_{cal} (Mg/m^3)	1.707	1.334
Abs. coeff.(mm^{-1})	4.090	1.972
2 θ range for data collection (°)	4.232 to 54	4.454 to 54
Reflections collected	81767	81767
Indep. Reflection, R(int)	7271, 0.0463	15113, 0.1040
Completeness of data	99.9 %	99.4 %
Data/ restraints / parameters	7271/0/395	15113/0/813
Goodness-of-fit on F^2	1.037	0.950
R1 [I>2sigma(I)], wR2	0.0159, 0.0386	0.0507, 0.1013
R1 (all data), wR2	0.0173, 0.0391	0.1070, 0.1156
Largest diff. peak and hole	0.78, -0.45	1.26, -1.12
(e • $Å^{-3}$)		

3. NMR spectra

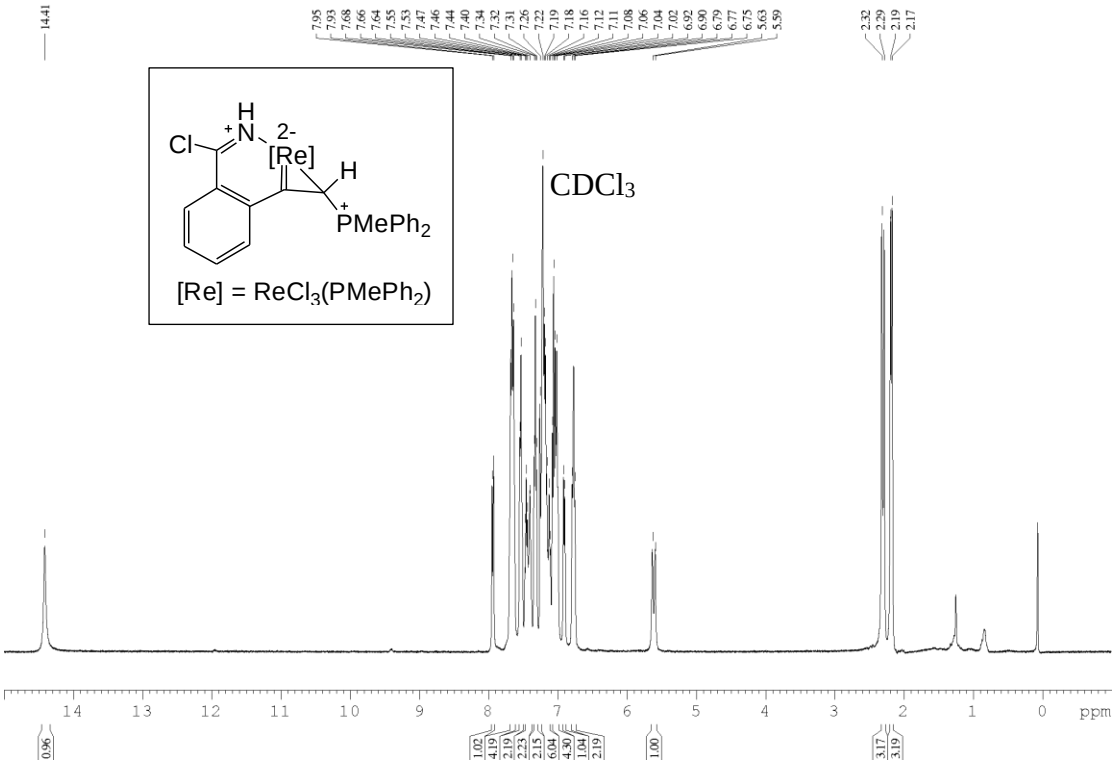

Figure S10. The ^{1}H NMR spectrum of complex **2** in $CDCl_3$ at 400.1 MHz.

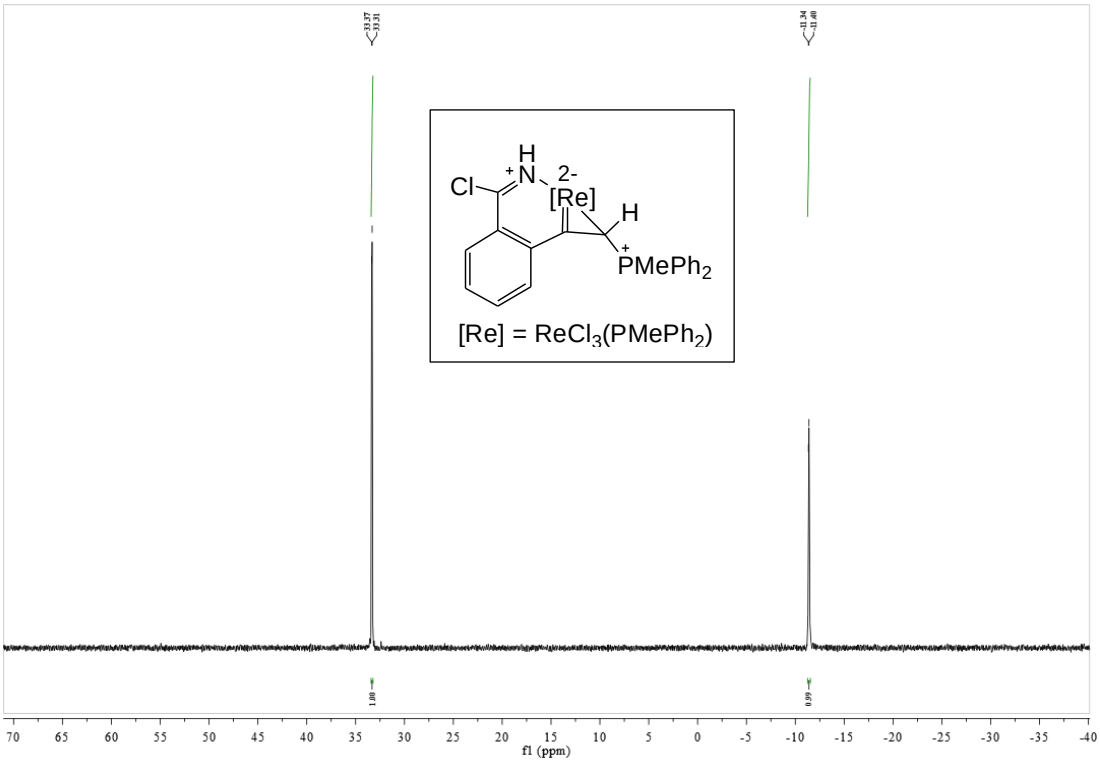

Figure S11. The $^{31}P\{^{1}H\}$ NMR spectrum of complex **2** in $CDCl_3$ at 162.0 MHz.

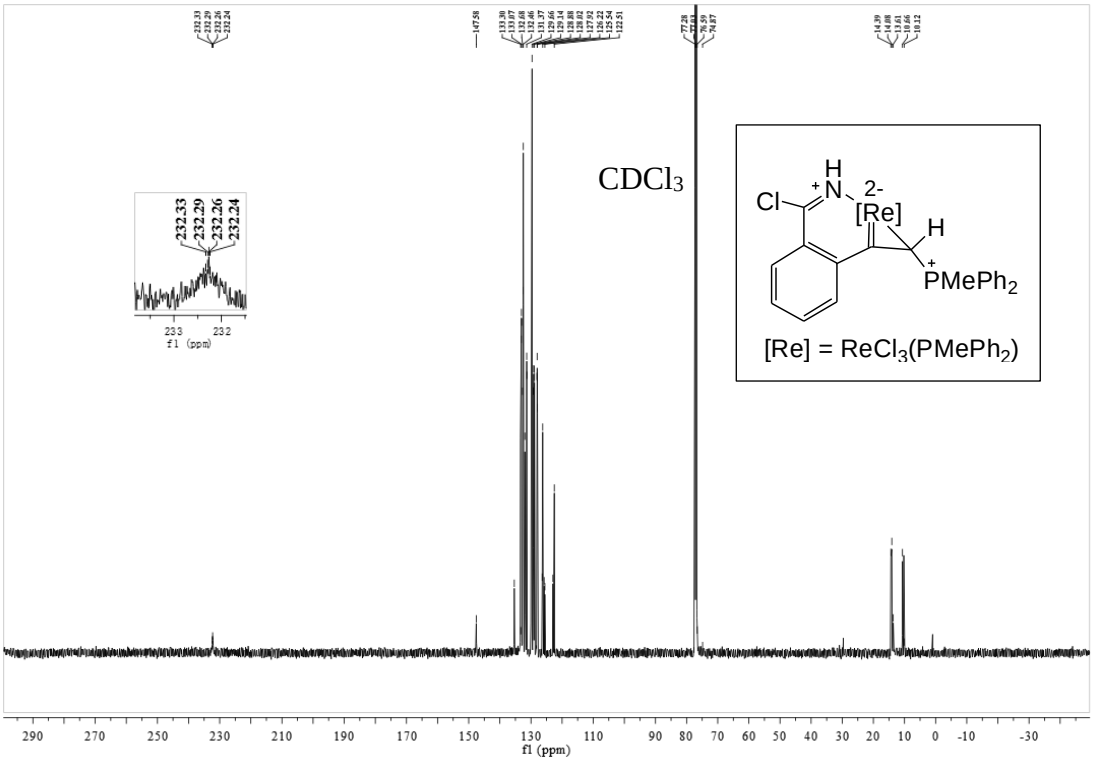

Figure S12. The $^{13}C\{^{1}H\}$ NMR spectrum of complex **2** in $CDCl_3$ at 100.6 MHz.

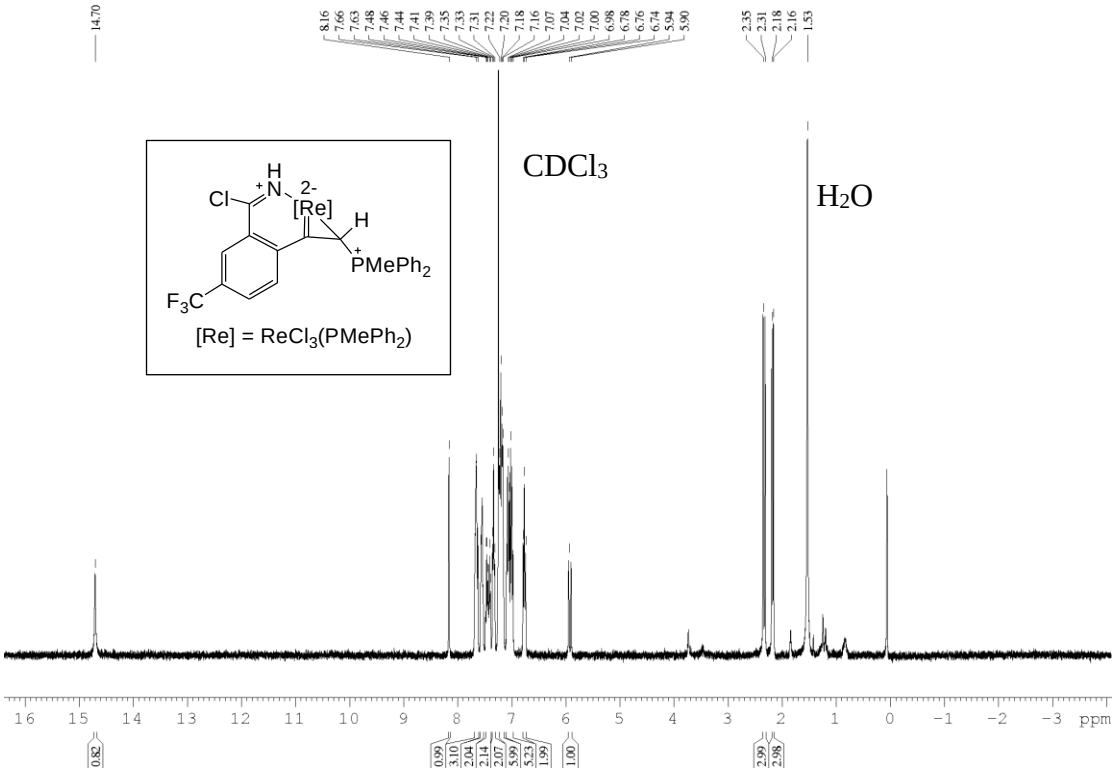

Figure S13. The ^{1}H NMR spectrum of complex **3** in $CDCl_3$ at 400.1 MHz.

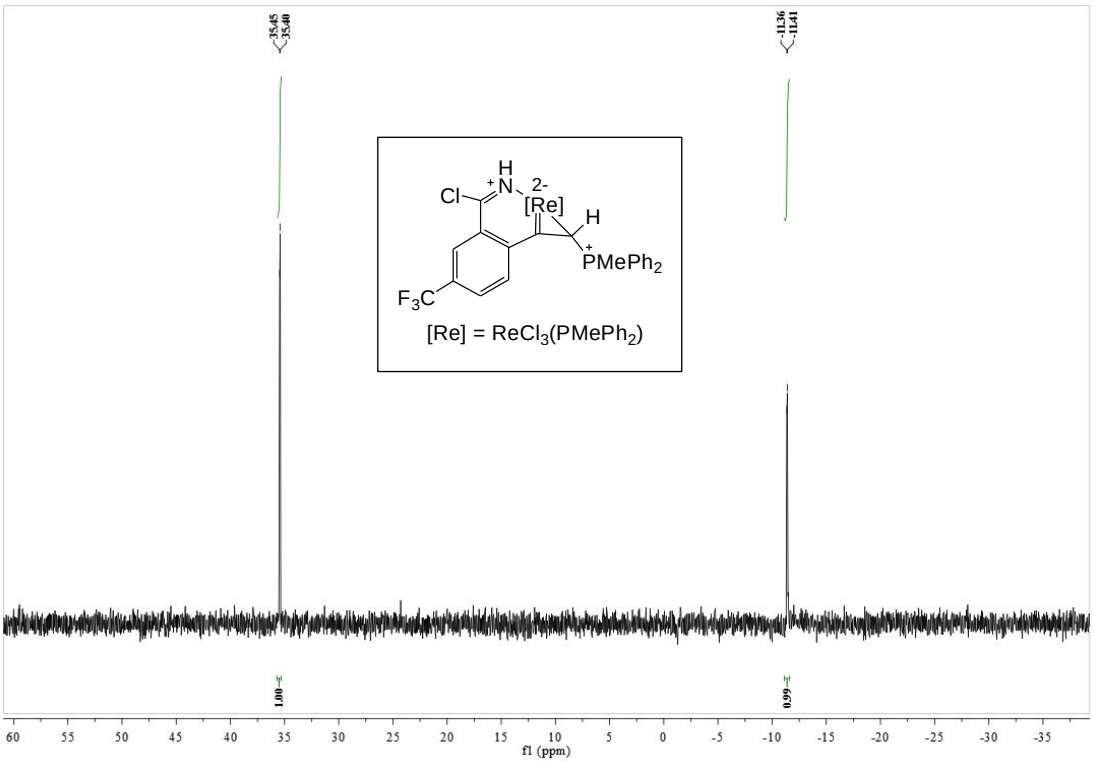

Figure S14. The $^{13}P\{^{1}H\}$ NMR spectrum of complex **3** in $CDCl_3$ at 162.0 MHz.

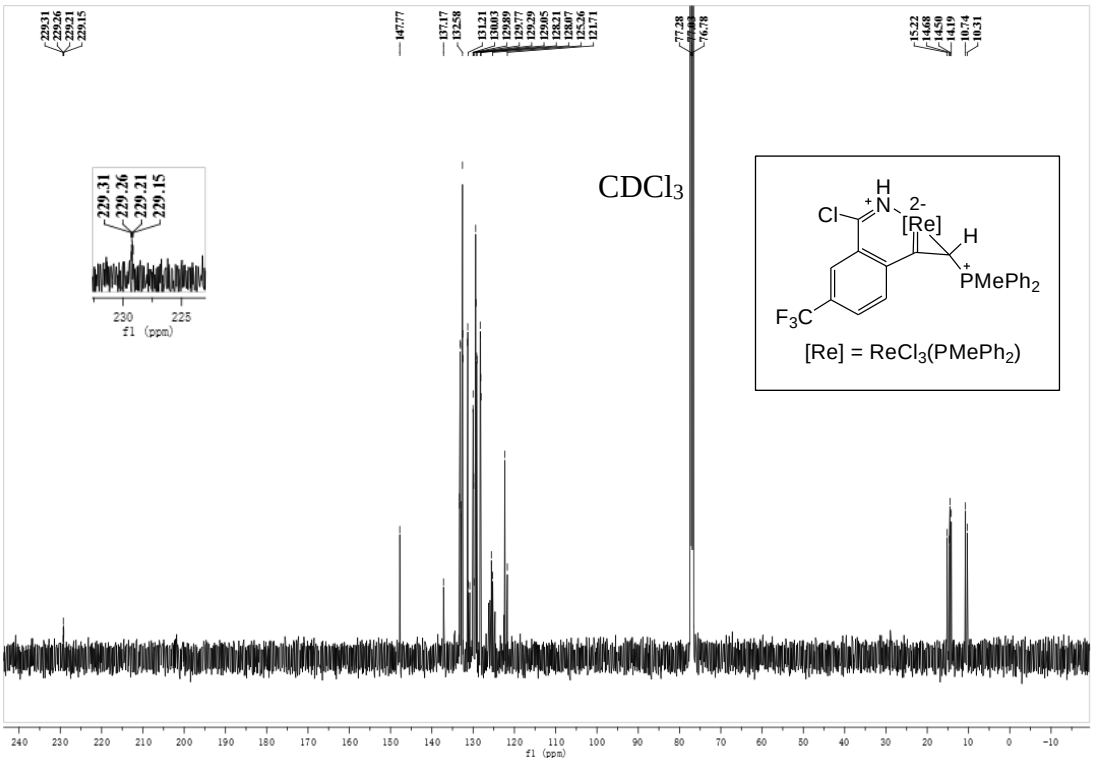

Figure S15. The $^{13}C\{^{1}H\}$ NMR spectrum of complex **3** in $CDCl_3$ at 100.6 MHz.

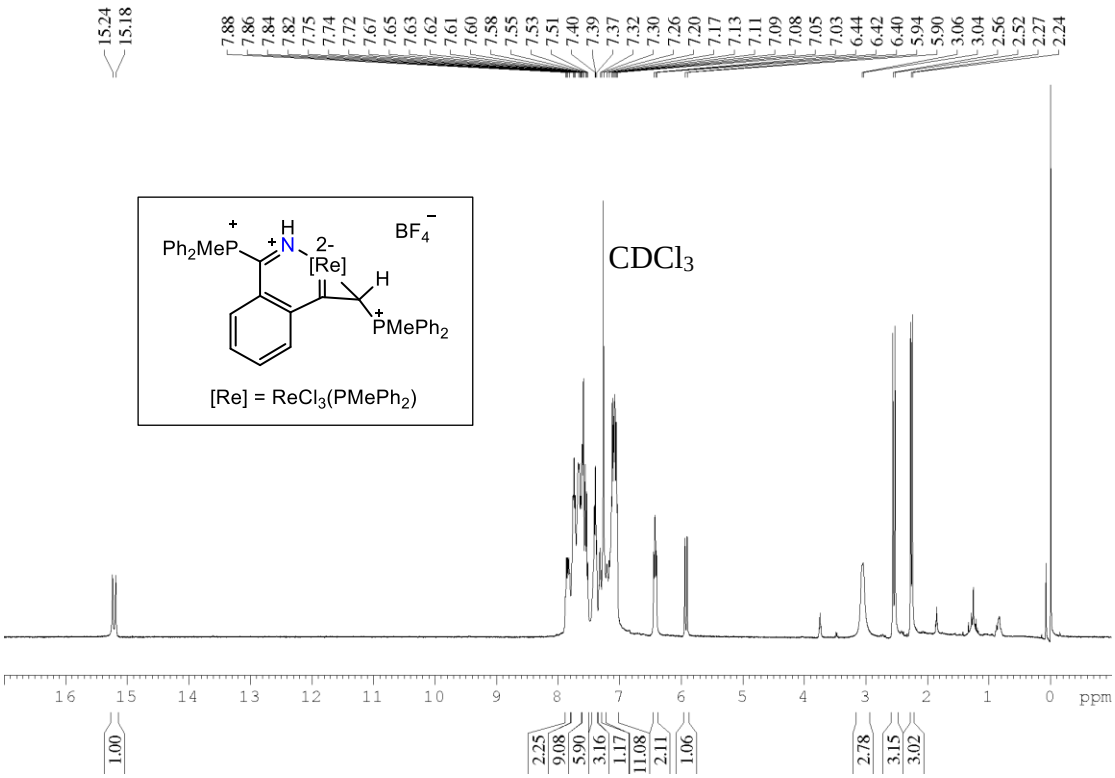

Figure S16. The ^{1}H NMR spectrum of complex **4** in $CDCl_3$ at 400.1 MHz.

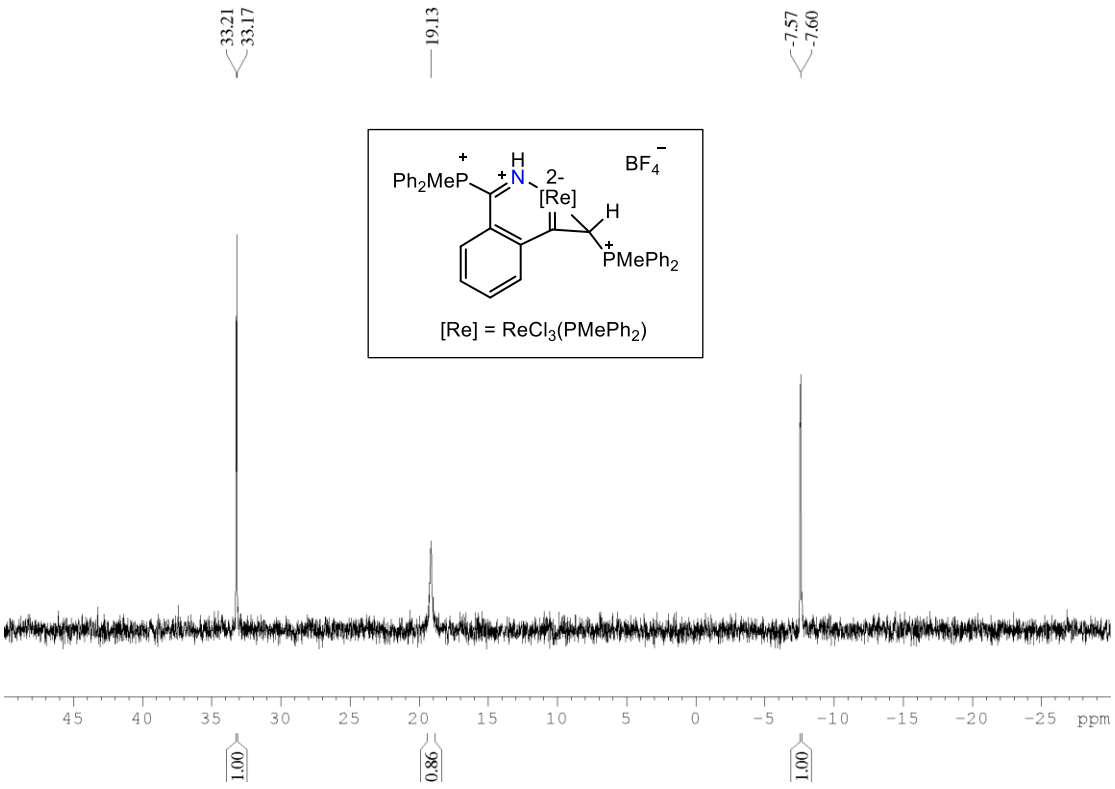

Figure S17. The $^{31}P\{^{1}H\}$ NMR spectrum of complex **4** in $CDCl_3$ at 162.0 MHz.

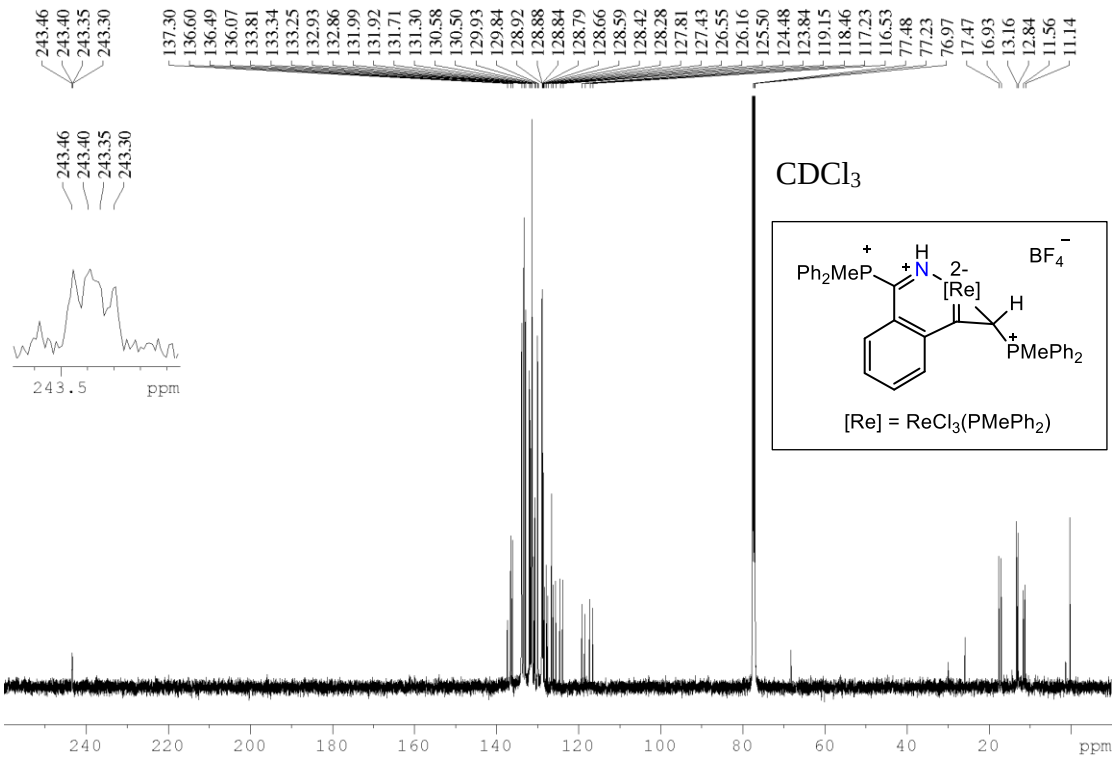

Figure S18. The $^{13}C\{^{1}H\}$ NMR spectrum of complex **4** in $CDCl_3$ at 100.6 MHz.

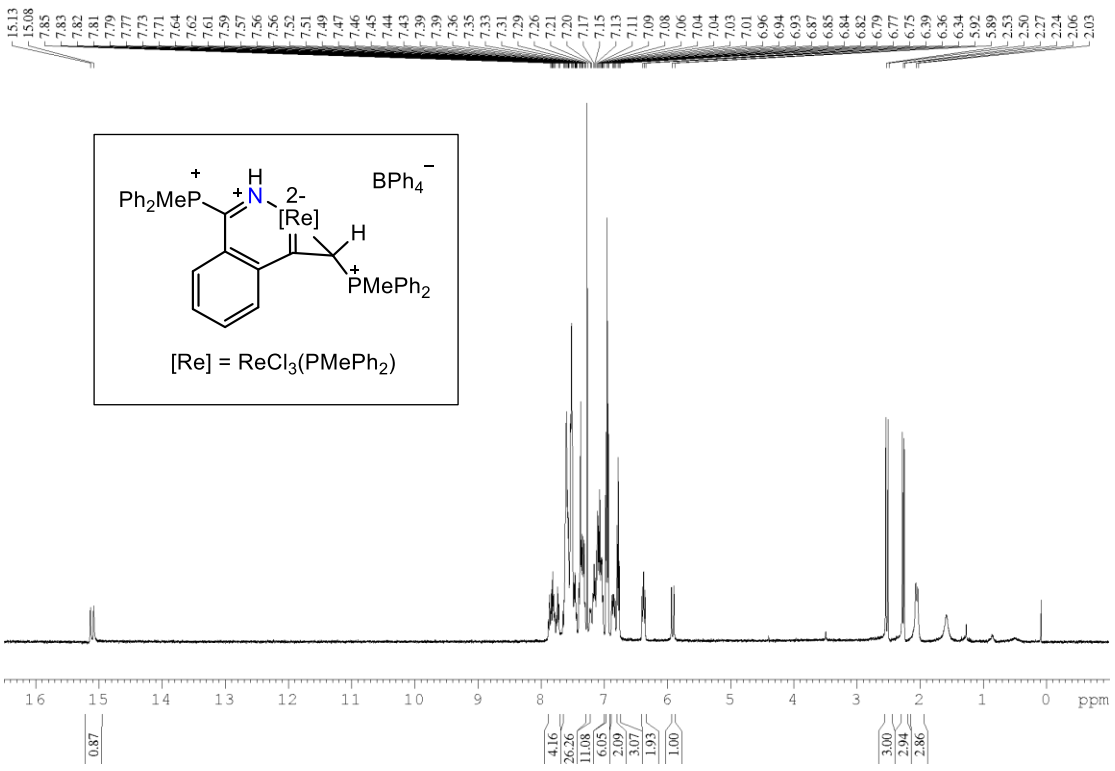

Figure S19. The ^{1}H NMR spectrum of complex **4^{+}(BPh_4^{-})** in $CDCl_3$ at 400.1 MHz.

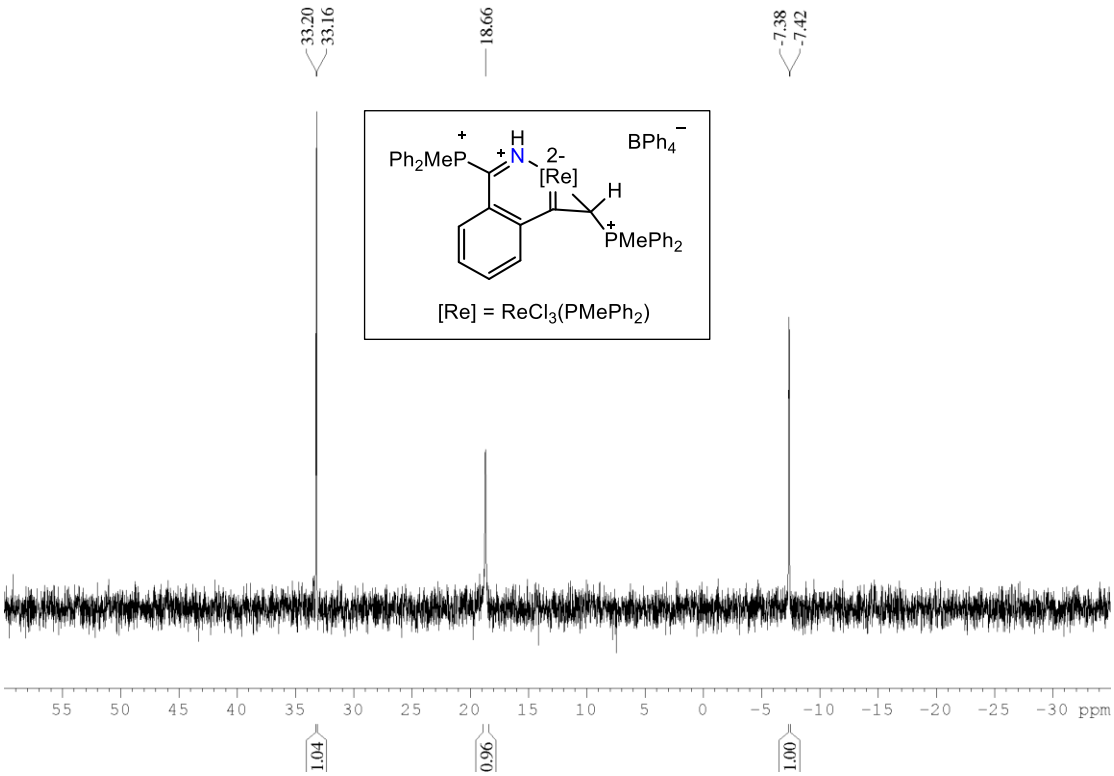

Figure S20. The $^{31}P\{^{1}H\}$ NMR spectrum of complex **$4^{+}(BPh_4^{-})$** in $CDCl_3$ at 162.0 MHz.

4. The Calculated Cartesian Coordinates with Electronic Energies

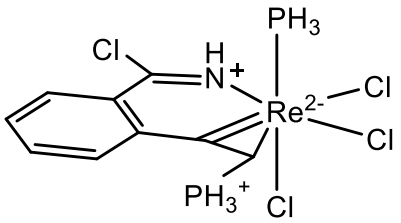

M-N

E = -3007.16424742 A.U.

Re	-0.87019600	-0.18586800	0.06406500
Cl	-1.93675600	-2.38463100	-0.39464800
Cl	-1.07846900	0.46374800	-2.30213500
Cl	-3.19729900	0.57996300	0.43109600
Cl	2.94852600	-2.77528300	-0.75054900
P	-0.98384200	3.01988900	-0.78311300
P	-1.08963100	-0.84984700	2.37094100
N	0.75004200	-1.41857100	-0.32832100
C	2.03769600	-1.32665100	-0.31725600
C	2.76607600	-0.13479700	0.02988800
C	2.02129600	1.03010700	0.37542700
C	0.60592200	0.98213300	0.38994400
C	-0.47866100	1.90029800	0.51281000
H	-0.81725500	2.28300800	1.47366900
C	4.16888000	-0.07089600	0.02810100
H	4.73977300	-0.95052500	-0.23211600
C	4.82323900	1.10157700	0.34860300
H	5.90575800	1.12951800	0.33958100
C	4.09696700	2.25142700	0.68131500
H	4.61730000	3.16806800	0.93090800
C	2.71914900	2.21279700	0.69329000
H	2.14703000	3.09280000	0.96162500
H	0.38716000	-2.33129500	-0.60830300
H	-2.26265200	-1.54515300	2.69510700
H	-0.12282800	-1.69752500	2.95275100
H	-1.11526600	0.16046100	3.35634600
H	-2.27337100	2.80936900	-1.27361200
H	-1.04363000	4.31463900	-0.23114200
H	-0.12089600	3.18556400	-1.86556400

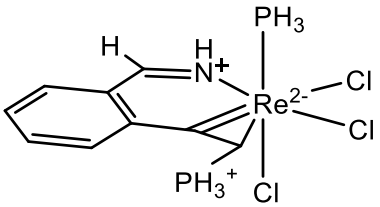

M-N-H

E = -2547.54276054 A.U.

Re	-0.73425100	-0.20001100	-0.00817100
Cl	-2.35636800	-1.90965700	-0.82089900
Cl	-0.86654500	1.01253100	-2.14956100
Cl	-2.77979900	0.99744300	0.74076100
P	-0.06656500	3.04553400	-0.12581300
P	-1.02379400	-1.30348900	2.11143500
N	0.48728200	-1.65769100	-0.80676100
C	1.76336300	-1.88509800	-0.90174700
C	2.76611800	-1.01331400	-0.37220300
C	2.38315900	0.18525800	0.28919100
C	1.00418700	0.47634900	0.42204700
C	0.18825700	1.56870500	0.84283100
H	-0.00561100	1.78646900	1.89145600
C	4.13022000	-1.31812300	-0.51172400
H	4.41814400	-2.23285100	-1.01767500
C	5.09617000	-0.46517600	-0.01831400
H	6.14479300	-0.71052900	-0.13336100
C	4.72376700	0.72182800	0.63003100
H	5.48691500	1.38753600	1.01467800
C	3.39043700	1.04121800	0.78014300
H	3.09829700	1.95187000	1.28985900
H	-0.10161800	-2.36712900	-1.24227600
H	-2.32023700	-1.75481900	2.39529300
H	-0.28180600	-2.46887600	2.40201500
H	-0.74953700	-0.57403200	3.28865600
H	-1.38486600	3.26808300	-0.52636100
H	0.22478300	4.15407900	0.69351100
H	0.76795500	3.24691600	-1.22440600
H	2.08806200	-2.78798700	-1.41222300

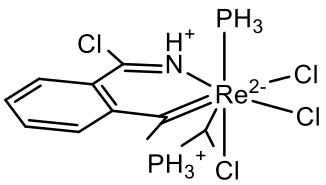

E = -3086.91200242 A.U.

Re	0.92526500	0.31609700	0.08007400
Cl	0.99824500	2.13966400	-1.78569700
Cl	2.99994200	-0.82211100	-0.85795900
Cl	2.17801700	2.12103700	1.22726400
P	0.34392500	-0.43495000	-2.14369800
P	0.86938000	-3.35320300	0.38069000
N	-0.57311600	1.62370200	0.65846600
H	-0.17398700	2.49542200	1.01677100
C	-0.35135400	-2.34768300	1.30087800
H	0.20557000	-2.05764700	2.18956300
C	-0.51479800	-1.03569500	0.48382300
C	-1.87362600	-0.82880000	-0.02877500
C	-2.55123300	0.42827700	0.05706600
C	-1.85058800	1.56767200	0.58561800
C	-2.58707600	-1.87486000	-0.66453900
H	-2.09620200	-2.82564800	-0.81963200
C	-3.86366000	-1.71459600	-1.15852200
H	-4.34860100	-2.53841500	-1.66900400
C	-4.52870100	-0.49495100	-1.00630300
H	-5.53693200	-0.36721300	-1.37878100
C	-3.87516100	0.55425900	-0.40135600
H	-4.36934100	1.51049000	-0.30430500
H	1.90031400	-2.57539900	-0.24114400
H	1.45204000	-4.36273600	1.16607000
H	0.20037600	-4.08551900	-0.60918700
H	0.12984100	-1.83305800	-2.29746900
H	-0.85702000	0.01373500	-2.71985600
H	1.27348600	-0.24717500	-3.16708100
C	-1.54060200	-3.18073300	1.81548300
H	-2.27224100	-2.50819000	2.26551000
H	-2.05869800	-3.76417300	1.05774900
H	-1.19869300	-3.86495800	2.59602100
C	1.87570200	-0.67156200	1.82508500
H	1.28303700	-0.49324900	2.72936600
H	2.09898900	-1.74097900	1.76133000
H	2.83547800	-0.18179100	1.94218500
Cl	-2.76934900	2.95950500	1.14941700

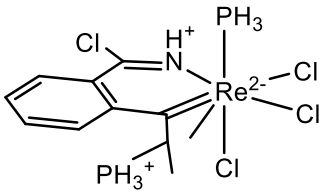

E = -3086.934689 A.U.

Cl	1.99041900	-2.66075500	-0.41080100
Cl	0.95005800	-0.88715500	2.26955300
Cl	2.63673300	1.18499300	0.54736900
P	2.46137800	-0.22331800	-1.89577400
P	0.75114400	2.66794500	1.90042700
C	-0.07514400	2.63826800	0.24836600
H	-0.98207800	3.20196600	0.47818500
C	-0.45410000	1.16273500	-0.07760500
C	-1.91934800	1.04939300	-0.31695000
C	-2.11061500	-1.35555400	0.41338400
C	-2.61514400	2.13216700	-0.90108000
H	-2.06599200	3.01784000	-1.18719500
C	-3.97156700	2.11404200	-1.16821300
H	-4.43601200	2.97569100	-1.63357000
C	-4.73231700	0.99938600	-0.83505900
H	-5.79862300	0.97577700	-1.01918900
C	-4.09827500	-0.09317500	-0.27994800
H	-4.67810800	-0.97168600	-0.03973100
H	2.60145800	1.00546400	-2.58165700
H	3.77898800	-0.44001900	-1.47987000
H	2.35117600	-1.09460500	-2.98787100
H	1.88817500	3.46741800	2.02169300
H	-0.16039300	3.37054000	2.71957000
H	0.89284500	1.42170800	2.53882000
Re	0.74084800	-0.38509600	-0.17421700
C	0.68530100	3.42048500	-0.83313400
C	-2.71390600	-0.11048000	-0.04472100
C	-0.18195800	-0.95286400	-2.13264400
H	0.08766700	3.42436600	-1.74658500
H	0.85021600	4.46081500	-0.53820200
H	1.64377700	2.96183900	-1.05595400
H	-1.26428500	-0.95860100	-2.03094700
H	0.05060000	-0.24598700	-2.93308700
H	0.15406200	-1.94634200	-2.42624800
N	-0.87382500	-1.63093500	0.32955600
H	-0.58205200	-2.55069600	0.65969700
Cl	-3.15624700	-2.60605700	1.09372500

References

[1] Gaussian 16, Revision A.03, M. J. Frisch, G. W. Trucks, H. B. Schlegel, G. E. Scuseria, M. A. Robb, J. R. Cheeseman, G. Scalmani, V. Barone, G. A. Petersson, H. Nakatsuji, X. Li, M. Caricato, A. V. Marenich, J. Bloino, B. G. Janesko, R. Gomperts, B. Mennucci, H. P. Hratchian, J. V. Ortiz, A. F. Izmaylov, J. L. Sonnenberg, D. Williams-Young, F. Ding, F. Lipparini, F. Egidi, J. Goings, B. Peng, A. Petrone, T. Henderson, D. Ranasinghe, V. G. Zakrzewski, J. Gao, N. Rega, G. Zheng, W. Liang, M. Hada, M. Ehara, K. Toyota, R. Fukuda, J. Hasegawa, M. Ishida, T. Nakajima, Y. Honda, O. Kitao, H. Nakai, T. Vreven, K. Throssell, J. A. Montgomery, Jr., J. E. Peralta, F. Ogliaro, M. J. Bearpark, J. J. Heyd, E. N. Brothers, K. N. Kudin, V. N. Staroverov, T. A. Keith, R. Kobayashi, J. Normand, K. Raghavachari, A. P. Rendell, J. C. Burant, S. S. Iyengar, J. Tomasi, M. Cossi, J. M. Millam, M. Klene, C. Adamo, R. Cammi, J. W. Ochterski, R. L. Martin, K. Morokuma, O. Farkas, J. B. Foresman, and D. J. Fox, Gaussian, Inc., Wallingford CT, 2016.

[2] a) A. D. Becke, *J. Chem. Phys.* 1993, **98**, 5648-5652; b) B. Miehlich, A. Savin, H. Stoll, H. Preuss, *Chem. Phys. Lett.* 1989, **157**, 200-206; c) C. Lee, W. Yang, R. G. Parr, *Phys. Rev. B.* 1988, **37**, 785-789.

[3] a) F. Weigend, R. Ahlrichs, *Phys. Chem. Chem. Phys.* 2005, **7**, 3297–3305; b) F. Weigend, *Phys. Chem. Chem. Phys.* 2006, **8**, 1057-1065.

[4] P. J. Hay, W. R. Wadt, *J. Chem. Phys.* 1985, **82**, 299-310.

[5] a) P. v. R. Schleyer, C. Maerker, A. Dransfeld, H. Jiao, N. J. R. v. E. Hommes, *J. Am. Chem. Soc.* 1996, **118**, 6317-6318; b) Z. Chen, C. S. Wannere, C. Corminboeuf, R. Puchta, P. v. R. Schleyer, *Chem. Rev.* 2005, **105**, 3842-3888; c) H. Fallah-Bagher-Shaidaei, C. S. Wannere, C. Corminboeuf, R. Puchta, P. v. R. Schleyer, *Org. Lett.* 2006, **8**, 863-866.

[6] a) R. Herges, D. Geuenich, *J. Phys. Chem. A* 2001, **105**, 3214-3220. a) D. Geuenich, K. Hess, F. Kçhler, R. Herges, *Chem. Rev.* 2005, **105**, 3758-3772.

[7] J. W. Storer, D. J. Giesen, C. J. Cramer, and D. G. Truhlar, *J. Comput.-Aided Mol. Des.* 1995, **9**, 87-110.

[8] C. M. Breneman, and K. B. Wiberg, *J. Comput. Chem.* 1990, **11**, 361-373.

[9] D. W. Szczepanik, RunEDDB, available at: http://eddb.pl/ runeddb/.

[10] D. W. Szczepanik, M. Andrzejak, K. Dyduch, E. Zak, M. Makowski, G. Mazur, and J. Mrozek, *Phys. Chem. Chem. Phys.* 2014, **16**, 20514-20523.

[11] a) T. Lu, F. Chen, *Acta Chim. Sinica* 2011, **69**, 2393-2406; b) T. Lu, F. Chen, *J. Comput. Chem.* 2012, **33**, 580-592.

[12] W. Humphrey, A. Dalke, K. Schulten, *J. Mol. Graphics* 1996, **14**, 33-38.